PAPER

High performance and nearly wake-up free $Hf_{0.5}Zr_{0.5}O_2$ ferroelectric capacitor realized by middle layer strategy with BEOL compatibility

To cite this article: Yin-Chi Liu *et al* 2025 *Nanotechnology* **36** 045205

IOP Publishing

Nanotechnology

Nanotechnology **36** (2025) 045205 (6pp)

https://doi.org/10.1088/1361-6528/ad8bcc

High performance and nearly wake-up free $Hf_{0.5}Zr_{0.5}O_2$ ferroelectric capacitor realized by middle layer strategy with BEOL compatibility

Yin-Chi Liu[1,2], Gen-Ran Xie[2], Ji-Ning Yang[2], Hao Zhang[2], Dmitriy Anatolyevich Golosov[3], Chenjie Gu[4], Bao Zhu[2,5], Xiaohan Wu[2,5], Hong-Liang Lu[2], Shi-Jin Ding[2,5] and Wenjun Liu[1,2,6,*]

[1] Shaoxin Laboratory, Shaoxing, Zhejiang 312000, People's Republic of China
[2] School of Microelectronics, Fudan University, Shanghai 200433, People's Republic of China
[3] Belarusian State University of Informatics and Radioelectronics, Minsk 220013, Belarus
[4] Department of Microelectronic Science and Engineering, School of Physical Science and Technology, Ningbo University, Ningbo 315211, People's Republic of China
[5] Jiashan Fudan Institute, Fudan University, Jiaxing, Zhejiang 314100, People's Republic of China
[6] Zhangjiang Fudan International Innovation Center, Fudan University, Shanghai 201203, People's Republic of China

E-mail: wjliu@fudan.edu.cn

Received 9 August 2024, revised 11 October 2024
Accepted for publication 28 October 2024
Published 8 November 2024

Abstract

$Hf_{0.5}Zr_{0.5}O_2$ (HZO) has drawn great attention owing to its excellent ferroelectricity, sub-10 nm scalability, and CMOS compatibility. With regard to increasingly restrict thermal budget and power consumption, conventional HZO films need further optimization to meet these demands. Here, we propose a middle layer (ML) strategy aiming to enhance ferroelectricity and inhibit wake-up effect of ferroelectric (FE) capacitors compatible with back-end of line under the low operating electric field. ZrO_2, HfO_2, and Al_2O_3 were integrated into HZO film as different MLs. Among them, the device with ZrO_2 ML achieves the excellent double remnant polarization ($2P_r$) of 41.7 μC cm^{-2} under the operating electric field of 2 MV cm^{-1}. Moreover, ultralow wake-up ratios of around 0.08 and 0.05 were observed under 2 MV cm^{-1} and 3 MV cm^{-1}, respectively. Additionally, the FE capacitor with ZrO_2 ML demonstrated an enhanced reliability characterizations, including a stable $2P_r$ of 40.7 μC cm^{-2} after 4.3×10^9 cycles. This work provides the perspective to optimize both the ferroelectricity and reliability, while maintains the ultralow wake-up ratio in HfO_2-based FE through ML engineering.

Keywords: back end of line, ZrO_2 middle layer, remnant polarization, low-field operation, wake-up free

* Author to whom any correspondence should be addressed.

1. Introduction

Neuromorphic computing, a technique inspired by the human brain, continues to propel the rapid advancement of artificial intelligence [1]. Owing to non-volatile and tunable properties, ferroelectric (FE) memory can be regarded as an ideal synaptic in neural network for achieving large-scale parallel processing and low-power pattern recognition [2]. However, conventional FE perovskite-structured materials, such as $BaTiO_3$ (BTO), $Pb(Zr,Ti)O_3$ (PZT), and $Sr_2Bi_2TaO_9$ (SBT), face significant challenges in integrated systems due to their incompatibility with the CMOS back-end of line (BEOL) process, which has substantially restricted their further implementation [3, 4].

In recent years, hafnium-based FE material has gained extensive attention for next-generation non-volatile memory applications, such as FE random-access memory, FE field-effect transistor, and FE tunnel junction [5]. Zr-doped hafnium-based ($Hf_{0.5}Zr_{0.5}O_2$, HZO) FE capacitors exhibit the great potential in artificial neural network. Their exceptional scalability and compatibility with advanced CMOS processes make them one of great candidates [6]. Yet, the further integration and application in advanced process nodes of hafnium-based memories require addressing several issues, including optimizing ferroelectricity, improving the reliability, and suppressing the wake-up effect of FE capacitors compatible with the BEOL process.

To tackle these issues, significant efforts have been carried out. Kim *et al* applied Al_2O_3 interlayer to control the grain size in HZO films, which alleviates the deterioration in thicker HZO films. Nonetheless, the FE capacitors were annealed at 600 °C that is incompatible with the BEOL process [7]. By introducing TiO_2 and SiO_2 interlayers into HZO films, Joh *et al* optimized the ferroelectricity of FE capacitors and achieved a double remnant polarization ($2P_r$) of approximately 30.2 μC cm^{-2}. Nevertheless, further refinement strategy is needed because of its high annealing temperature (600 °C) and severe wake-up effect observed from endurance characteristics [8]. It is believed that the suppression of the interfacial defects by seed layers is the feasible approach to fabricate wake-up free devices [9]. Regarding to the operating electric field (3 MV cm^{-1}) and annealing temperature (450 °C), there remains room for improvement. With the help of superlattice structure, wake-up free devices are fulfilled, while the large leakage current, complex fabrication process, and high annealing temperature of 600 °C hinder extensive practical implementation [10]. Liu *et al* increased the proportion of FE phases within the Al-doped HfO_2-based FE thin film through a ZrO_2 regulating layer, resulting in a weaker wake-up effect and enhanced ferroelectricity ($2P_r \sim 31.2$ μC cm^{-2}). However, the operating electric field (>3 MV cm^{-1}) failed to align with the requirements for application in advanced process nodes [11]. The enhancement of ferroelectricity in HZO film by introducing ZrO_2 middle layer (ML) is verified, accomplishing excellent endurance exceeding 10^{10} cycles and $2P_r$ of ~39.6 μC cm^{-2}, the research on wake-up effect of FE capacitors and temperature dependent ferroelectricity was not conducted yet [12]. Hence, it is particularly vital to construct an HZO FE capacitor with a low operating electric field, wake-up free, and compatible with the BEOL process as well. More specific device parameters and process conditions of mentioned above are digested in table 1. In this work, we have incorporated MLs into the FE capacitor to achieve its low electric field operation, wake-up free, and BEOL compatibility. Various MLs, including ZrO_2, HfO_2, and Al_2O_3, were inserted into conventional HZO films to form HZO/ML/HZO stacks. The impacts of these MLs on the performance of FE capacitor were evaluated by varying operating electric fields and annealing temperatures. The FE capacitor with ZrO_2 ML achieved $2P_r$ of 41.7 μC cm^{-2} and 55.3 μC cm^{-2} under 2 MV cm^{-1} and 4 MV cm^{-1}, respectively. The $2P_r$ of 40.7 μC m^{-2} was maintained after endurance of 4.3×10^9 cycles demonstrating its superior endurance.

2. Experiment

The key process flows and schematics of FE capacitors with and without 1 nm ML are described in figures 1(a) and (b) and figures 1(c) and (d), respectively. Firstly, a 50 nm Tungsten (W) was deposited onto the SiO_2/p-Si substrate as the bottom electrode by utilizing physical vapor deposition (PVD). Then, plasma enhanced atomic layer deposition (PEALD) was applied to build the stack structure in sequence at 280 °C, i.e. 5 nm HZO/ 1 nm ML/5 nm HZO. For the capacitor without ML, only 10 nm HZO film was prepared directly. $Hf[N(CH_3)_2]_4$, $Zr[N(CH_3)_2]_4$, and oxygen plasma served as Hf, Zr, and oxygen sources, respectively. The growth rate of HfO_2 and ZrO_2 films is 0.14 nm/cycle for the PEALD process and the ALD cycle ratio of HfO_2/ZrO_2 is fixed at 1:1 during HZO deposition. The sputtering and patterning procedures were adopted to form 50 nm tungsten (W) top electrodes with 80×80 μm^2 contact region via PVD and photolithography. Finally, the FE capacitors were placed in nitrogen atmosphere and annealed at 350 °C, 450 °C and 500 °C using rapid thermal annealing. The transmission electron microscopy (TEM) was utilized to examine the micro-structure and elemental distribution of FE capacitors, the electrical measurement was performed on semiconductor analyzer (Agilent B1500A) and FE test system (Radiant, Precision Premier II).

3. Results and discussion

Figures 2(a)–(f) present the polarization-electric field (*P–E*) characteristics of FE capacitors without and with different MLs annealed at 350 °C, 450 °C and 500 °C under 2 MV cm^{-1} and 4 MV cm^{-1}. The ferroelectricity of FE capacitors varies after annealing at different temperatures. Meanwhile, the influence of electric fields on P_r is evident, as the high electric field of 4 MV cm^{-1} minimizes differences in P_r while low electric field of 2 MV cm^{-1} accentuate these discrepancies. In figure 2(a), FE capacitor with Al_2O_3 ML shows an incomplete FE hysteresis loop under 2 MV cm^{-1} with the annealing temperature of 500 °C. As the annealing temperature further decreases, its ferroelectricity disappears. Figure 2(a) and

Table 1. Summary of electric parameters and annealing temperature of reference devices.

Ref.	Material	Electric parameters: $2P_r$ (μC cm^{-2})	Operating electric field(MV cm^{-1})	Wake-up free	Annealing temperature(°C)
[7]	Al_2O_3	31.2	4	N/A	500
[8]	TiO_2	30.2	3	N/A	500
	SiO_2	17.2			
[9]	ZrO_2	16.3	2.5/3	×	450
	HfO_2	23.8		×	
	Al_2O_3	14		×	
	TiO_2	29.3		√	
[10]	HfO_2/ZrO_2	27.4	2.5	√	500/600
[11]	ZrO_2	31.2	> 3	×	400

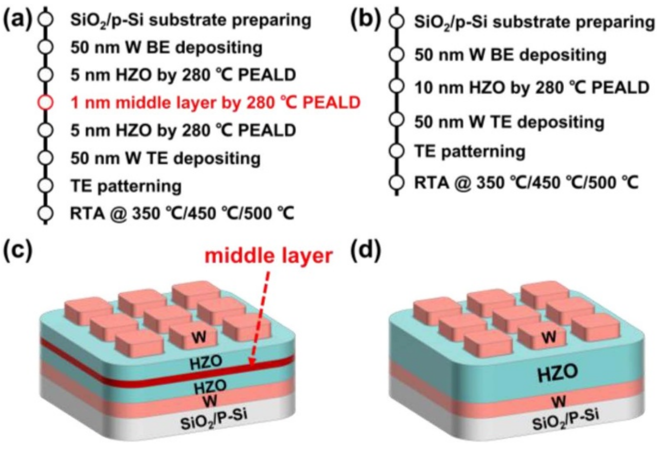

Figure 1. (a)and(b) Process flows and (c)and(d) schematics of FE capacitors with and without ML.

(b) demonstrate the FE capacitor without ML performs normally when annealed at temperatures above 450 °C. However, it experiences a significant decline in P_r after the annealing temperature drops 350 °C as depicted in figure 2(c). Simultaneously, the enhancement in ferroelectricity by inserting MLs is reflected at low annealing temperatures of 350 °C. The FE capacitors with HfO_2 and ZrO_2 MLs manifest better ferroelectricity compared to the FE capacitor without ML. Particularly the FE capacitor with ZrO_2 ML, it has a superior ferroelectricity at all annealing temperatures, showing the highest P_r among all capacitors. Under an electric field of 4 MV cm^{-1}, FE capacitors, except those with Al_2O_3 ML, exhibit similar performance since that the most of FE domains are able to switch under high electric field, as illustrated in figures 2(d)–(f). Consistent with the observation of low electric field, the FE capacitor with Al_2O_3 ML shows no ferroelectricity after annealing at 350 °C and 450 °C. It merely exhibits a weaker ferroelectricity at 500 °C. Moreover, its ferroelectricity is significantly affected by the electric field strength. This impact is evident from the FE hysteresis loops with dependence of the electric field.

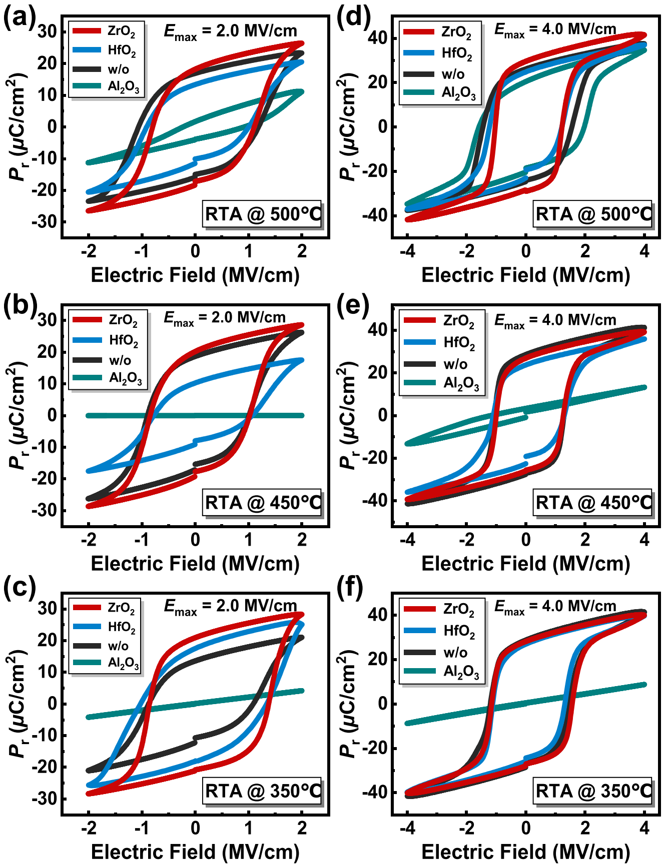

Figure 2. The *P–E* hysteresis loops of FE capacitors without and with different MLs annealed at (a) 500 °C, (b) 450 °C, and (c) 350 °C under the operating electric fields of 2 MV cm^{-1}, respectively. The *P–E* hysteresis loops of FE capacitors without and with different MLs annealed at (d) 500 °C, (e) 450 °C, and (f) 350 °C under the operating electric field of 4 MV cm^{-1}, respectively.

Figures 3(a)–(f) illustrate the $2P_r$ and the coercive electric field (E_c) extracted from the *P–E* hysteresis loops which are depicted in figures 2(a)–(f), shedding light on the FE behaviors of FE capacitors after integrating different MLs. Figures 3(a) and (b) provide the $2P_r$ and E_c of four FE capacitors at the

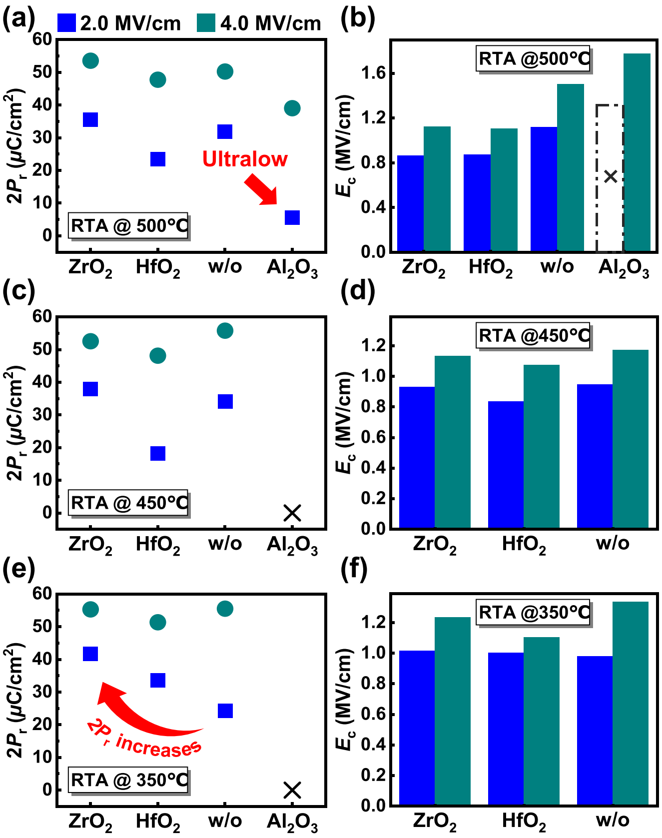

Figure 3. The extracted $2P_r$ of FE capacitors without and with different MLs annealed at (a) 500 °C, (c) 450 °C, and (e) 350 °C under the operating electric fields of 2 MV cm^{-1} and 4 MV cm^{-1}. The extracted E_c of FE capacitors without and with different MLs annealed at (b) 500 °C, (d) 450 °C, and (f) 350 °C.

annealing temperature of 500 °C, respectively. The performance of FE capacitor with Al_2O_3 ML is aligned with previous discussions, as indicated by the ultralow $2P_r$ of 5.6 μC cm^{-2} and 29.8 μC cm^{-2} measured at 2 MV cm^{-1} and 4 MV cm^{-1}, respectively. It is believed that Al_2O_3 has difficulty in crystallization at low temperature, which explains shows no ferroelectricity after annealed at 450 °C and 350 °C [13]. At the annealing temperature of 500 °C, the insertion of HfO_2 and ZrO_2 MLs leads to the decline of E_c, especially under the high electric field. Similarly, such decline in E_c also can be observed at the annealing temperature of 450 °C. In figure 3(a) and (c), under the electric field of 2 MV cm^{-1}, $2P_r$ of FE capacitor without under the operating electric fields of 2 MV cm^{-1}, and 4 MV cm^{-1}.ML are 34 μC cm^{-2} and 31.8 μC cm^{-2} at annealing temperatures of 450 °C and 500 °C, respectively. Nevertheless, a notable decrease in ferroelectricity occurs as the annealing temperature is decreased to 350 °C, with $2P_r$ dropping to 24.2 μC cm^{-2}. This significant deterioration could be linked to a reduced proportion of FE phases in the films annealed at 350 °C. As shown in figures 3(c) and (d), the effect of MLs on reducing E_c further weakens as the annealing temperatures decreases. In figures 3(e) and (f), under the electric of 2 MV cm^{-1}, the FE capacitor with ZrO_2 ML deliveries the highest $2P_r$ of 41.7 μC cm^{-2}, follows by the capacitor with HfO_2 ML, which $2P_r$ is 33.6 μC cm^{-2}. Under 2 MV cm^{-1}, the E_c of the capacitor without ML is 0.98 MV cm^{-1}. In comparison, the E_c for FE capacitors with ZrO_2 and HfO_2 MLs are 1.01 MV cm^{-1} and 1.00 MV cm^{-1}, respectively. Compared the FE capacitor without ML, it is verified that the insertion of MLs greatly improve the ferroelectricity of FE capacitors under the conditions of low annealing temperature and low electric field. This improvement is ascribed to the insertion of the MLs, which introduces additional tensile stress and promotes the transition from the non-FE phase to the FE phase [11, 14]. Figures 4(a)–(d) depict the cross-section TEM images of FE capacitors with different MLs. It is observed that FE capacitors without and with HfO_2 and ZrO_2 MLs annealed at 350 °C exhibit a distinct polycrystalline nature, whereas the FE capacitor with Al_2O_3 ML remain amorphous after annealing at 350 °C. Enhanced crystal nature of FE capacitor with ZrO_2 ML is presented in figure 4(d). Through fast Fourier transformation (FFT) analysis, we identified a distinct o- phase (111) with a d-spacing of 2.91 Å in FE films. Figure 4(e) displays the HAADF image of the FE capacitor with ZrO_2 ML and the EDS distribution mapping of all the elements along the corresponding position, showing the distributed Zr, Hf, O and W elements. The distribution and concentration of Zr and Hf elements indicate the presence of the ZrO_2 ML.

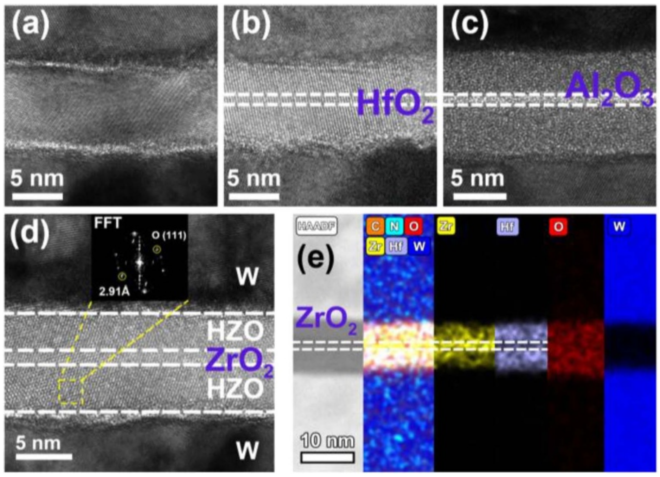

Figure 4. (a)–(d) Cross-sectional TEM images of FE capacitors without and with HfO_2, Al_2O_3 and ZrO_2 ML annealed at 350 °C. The inset shows the FFT and d-spacing of o—phases. (e) The HAADF and EDS results that characterize the distribution of Zr, Hf, O, and W atoms in the FE capacitor with ZrO_2 ML.

Figure 5(a) shows the wake-up ratios (1-$2P_{r\_initial}$/$2P_{r\_max}$) for FE capacitors without and with ZrO_2 or HfO_2 MLs under 2 MV cm^{-1} and 3 MV cm^{-1}. Here, $2P_{r\_initial}$ refers to the polarization measured under the pristine state of FE capacitors, and $2P_{r\_max}$ is measured under the state of FE capacitors after applying 10^4 cycles of wake-up pulse. Under 2 MV cm^{-1}, the average wake-up ratio of FE capacitors with ZrO_2 ML at 0.08, as shown in figure 5(a). However, FE capacitors with HfO_2 ML and without MLs have high wake-up ratios, both approximately at 0.19. As the electric field increases to 3 MV cm^{-1}, the wake-up effect in FE capacitors with ZrO_2 ML is further suppressed, with its wake-up ratio shrinking to 0.05. Such declining tendency is also observed

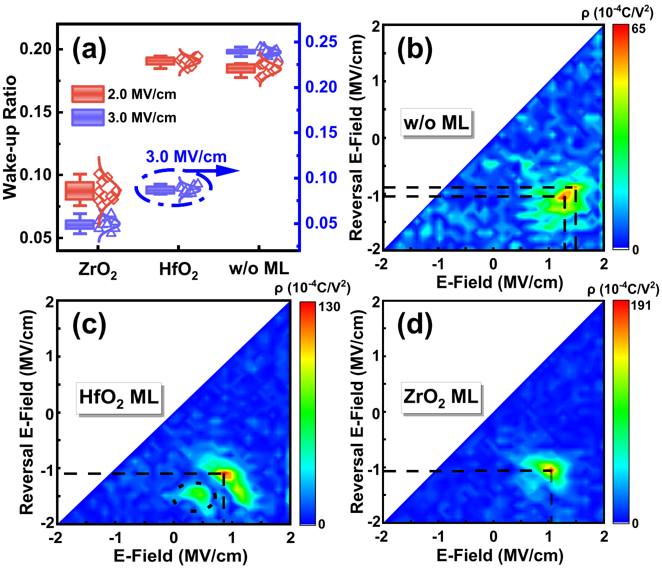

Figure 5. (a) The wake-up ratios ($1–2P_{r\_initial}/2P_{r\_max}$) for FE capacitors without and with ZrO_2 or HfO_2 MLs under 2 MV cm^{-1} and 3 MV cm^{-1}. First-order reversal curve (FORC) diagrams of FE capacitors (b) without ML, (c) with HfO_2 ML and (d) ZrO_2 ML under the electric field ranging from -2 MV cm^{-1} to 2 MV cm^{-1}. Note that the wake-up ratios are derived from 10 devices of each sample annealed at 350 °C.

in FE capacitor with HfO_2 ML, where the wake-up ratio drops from 0.19 to 0.08. Conversely, the wake-up ratio of FE capacitor without ML not fall but rises to 0.24. First-order reversal curve (FORC) diagrams are used to characterize the switching behavior of ferroelectric domains within ferroelectric films, as shown in figures 5(b)–(d). In figure 5(b) the first-order reversal curve (FORC) diagram of the FE capacitor without ML is depicted, with the electric fields ranging from -2 MV cm^{-1} to 2 MV cm^{-1}. Compared to the FE capacitor with ZrO_2 ML, a lower peak density in the capacitor without MLs indicates fewer FE domains switching at an operating electric field of 2 MV cm^{-1}, which corresponds to the $2P_r$ of the P–V loop in figure 2(c). On the other hand, as shown in figure 5(c), the splitting of domain peaks in FE capacitor with HfO_2 ML indicates the uneven distribution of oxygen vacancies within the FE film, causing FE domains to be pinned. This is regarded as the primary cause of the wake-up effect in HZO/HfO_2/HZO stack films [15–17]. Moreover, oxygen vacancies near the interface induce the internal built-in field, thereby hindering the switching of FE domains under low electric fields. Figure 5(d) shows the FORC diagram of the FE capacitor with ZrO_2 ML in the pristine state. The presence of single switching density peak in the FORC diagram suggests that oxygen vacancies in the HZO film tend to more uniformly distribute after inserting ZrO_2 ML, thereby the wake-up effect can be substantially suppressed.

Figure 6(a) presents the FE capacitor with HfO_2 ML has severe fatigue phenomenon driven by low electric field of 1.5 MV cm^{-1} with the frequency of 1 MHz. The device without ML shows a low $2P_r$ window, and its $2P_r$ drops below 15 μC cm^{-2} after 1.8×10^7 cycles. Figure 6(b) displays the

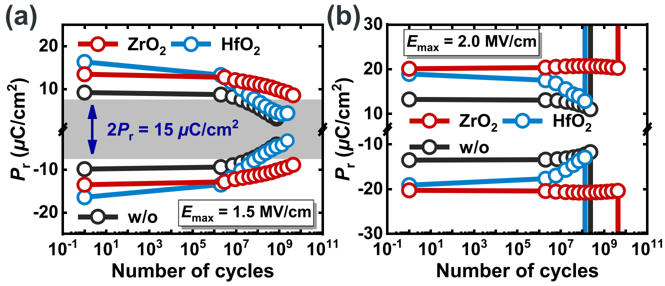

Figure 6. The endurance characteristics of capacitors without and with HfO_2 or ZrO_2 MLs under the operating electric field of (a) 1.5 MV cm^{-1} and (b) 2 MV cm^{-1}.

endurance characteristic of devices under the electric field of 2 MV cm^{-1}. Remarkably, the FE capacitor with ZrO_2 ML has a stable $2P_r$ of 40.7 μC cm^{-2} after enduring 4.3×10^9 cycles, while the other capacitors breakdown earlier. The enhancement in reliability is attributed to the insertion of ZrO_2 ML has interrupted the continuous growth of grains and segmented the grain boundaries, which slowed down the formation of the breakdown paths during cycling, thereby improving the reliability of the device [12, 18].

4. Conclusion

In summary, we have demonstrated a nearly wake-up free FE capacitor annealed at 350 °C with the low operating electric field enabled by ZrO_2 ML engineering. Compared to the capacitors without and with HfO_2 ML, the FE capacitor with ZrO_2 ML annealed at 350 °C exhibits an enhanced $2P_r$ of 41.7 μC cm^{-2} under the electric field of 2 MV cm^{-1}. Additionally, ultralow wake-up ratios of approximately 0.08 and 0.05 were obtained at 2 and 3 MV cm^{-1} respectively. Such improved ferroelectricity and reduced wake-up ratio are associated with the uniformly distributed oxygen vacancies and concentratedly switched FE domains in the capacitor with ZrO_2 ML. Furthermore, the FE capacitor with ZrO_2 ML shows competitive reliability of a $2P_r$ of 40.7 μC cm^{-2} after 4.3×10^9 cycles. These findings suggest that the insertion of ZrO_2 ML as a strategy is an effective solution to realize BEOL compatible, low-field operational and wake-up free FE devices.

Data availability statement

All data that support the findings of this study are included within the article (and any supplementary files).

Acknowledgments

Yin-Chi Liu and Gen-Ran Xie contributed equally to this work. This work was supported by National Key Research and Development Program of China under Grant 2021YFB3202500, and Shanghai Municipal Science and Technology Commission under Grant 23511102300.

ORCID iDs

Ji-Ning Yang https://orcid.org/0009-0006-3020-7696
Chenjie Gu https://orcid.org/0000-0002-1339-4534
Hong-Liang Lu https://orcid.org/0000-0003-2398-720X
Shi-Jin Ding https://orcid.org/0000-0002-5766-089X
Wenjun Liu https://orcid.org/0000-0003-4217-8838

References

[1] Hassabis D, Kumaran D, Summerfield C and Botvinick M 2017 *Neuron* **95** 245–58
[2] Kim D, Heo S J, Pyo G, Choi H S, Kwon HJ and Jang J E 2021 *IEEE Access* **9** 140975–82
[3] Setter N *et al* 2006 *Phys. J. Appl. Phys.* **100** 051606
[4] Mikolajick T, Slesazeck S, Mulaosmanovic H, Park M H, Fichtner S, Lomenzo P D, Hoffmann M and Schroeder U 2021 *Phys. J. Appl. Phys.* **129** 100901
[5] Xiao Y, Deng S, Zhao Z, Faris Z, Xu Y, Huang TJ, Narayanan V and Ni K 2023 *IEEE Electron Device Lett.* **44** 1436–9
[6] Zheng Q, Wang Z, Gong N, Yu Z, Chen C, Cai Y, Huang Q, Jiang H, Xia Q and Huang R 2019 *IEEE Electron Device Lett.* **40** 1309–12
[7] Kim H J, Park M H, Kim Y J, Lee Y H, Jeon W, Gwon T, Moon T, Kim K D and Hwang C S 2014 *Appl. Phys. Lett.* **105** 192903
[8] Joh H, Jung T and Jeon S 2021 *IEEE Trans. Electron Devices* **68** 2538–42
[9] Li X, Wu J, Tai L, Dou X, Sang P, Xu H, Zhan X, Wang X and Chen J 2023 *IEEE Trans. Electron Devices* **71** 1035–48
[10] Bai N *et al* 2022 *Adv. Electron. Mater.* **9** 2200737
[11] Liu Y *et al* 2023 *Adv. Electron. Mater.* **9** 2300208
[12] Liu YC *et al* 2024 *IEEE Electron Device Lett.* **45** 388–91
[13] Jakschik S, Schroeder U, Hecht T, Gutsche M, Seidl H and Bartha J W 2003 *Thin Solid Films* **425** 216–20
[14] Nie B *et al* 2023 *IEEE Electron Device Lett.* **44** 1456–9
[15] Jiang P, Luo Q, Xu X, Gong T, Yuan P, Wang Y, Gao Z, Wei W, Tai L and Lv H 2020 *Adv. Electron. Mater.* **7** 2000728
[16] Chen L, Liang Z, Shao S, Huang Q, Tang K and Huang R 2023 *Nanoscale* **15** 7014–22
[17] Zhou Y, Zhang Y K, Yang Q, Jiang J, Fan P, Liao M and Zhou Y C 2019 *Comput. Mater. Sci.* **167** 143–50
[18] Tai L *et al* 2023 *IEEE Electron Device Lett.* **44** 753–6